Turbulent Saturation of Tokamak-Core Zonal Flows

K. Hallatschek

Centre for Interdisciplinary Plasma Science, Max-Planck Institut für Plasmaphysik, EURATOM-IPP Association, D-85748 Garching, Germany

(Received 3 September 2003; published 2 August 2004)

Current theories of zonal flow dynamics focus on the transport of poloidal momentum. Different from a cylinder, stationary poloidal flows in a tokamak are accompanied by (possibly kinetic) flows *along* the magnetic field, which maintain incompressibility, and comprise the major part of the flow energy. In numerical turbulence studies, the flows saturate by the turbulent diffusion of the *parallel* flow, whereas the poloidal momentum transport continues to strongly drive the flows.

DOI: 10.1103/PhysRevLett.93.065001 PACS numbers: 52.35.Ra, 52.55.Fa, 52.65.Kj

Introduction.—The turbulence level of the ion temperature gradient (ITG) modes, dominating in the core of modern magnetic confinement devices, is controlled by the shearing action of zonal flows (ZF) [1–4], electric potential perturbations of zero poloidal and toroidal mode number. ZFs cause a poloidal $E \times B$ drift, which is radially varying but constant on a flux surface. Elimination of ZFs in turbulence computations was found to raise anomalous diffusivities a factor 10–100 above usual mixing length estimates. The excitation and damping of these flows is a topic of current research, which in the end might lead to an understanding of the intriguing and practically important internal and high-confinement-mode transport barriers.

So far, this exploration has focused on poloidal turbulence forces: ZFs are thought to be excited by variations of the perpendicular Kelvin-Helmholtz instability [5,6] of the ITG modes. In several experiments, the flow drive by poloidal Reynolds stress has been measured [7,8]. Analytically, a saturation of the flows caused by a reduction of the poloidal ZF drive and collisional damping [4] has been predicted. In simulations, the collisional ZF damping near marginality [1] has been studied, and a collisionless instability acting perpendicular to the magnetic field has been found, which can destroy the ZFs [9].

However, the ZFs are not simply poloidal flows: Their free energy (or effective inertia) is several times larger than that of a purely poloidal flow [3]. The underlying hidden ZF component is best understood in a fluid framework: Stationarity of the flows forbids plasma compression. Hence, perpendicular flows in a curved or inhomogeneous magnetic field require additional flows parallel to the field, which cancel their divergence. These are not a small correction: The strong magnetic field along the plasma column makes the connection distance along a field line between two oppositely curved regions (e.g., $\pi q R$, $q > 1$ in a tokamak) a major detour. Therefore, the parallel flow is actually larger than the poloidal flow.

The turbulent forces on the poloidal and the dominant parallel flow components are investigated below in 3D electrostatic fluid ITG turbulence computations. The chosen model is sufficient to observe these effects, yet it is simple and comparable with a large body of simulations.

Model equations.—The ITG turbulence is described by the equations of [10], with the additional approximations of adiabatic electrons (due to the high electron thermal velocity) and local conditions (due to low $\rho^* = \rho_i/a$, high parameter λ in Ref. [10]). The system for the fluctuation quantities ϕ, T_i, $v_\parallel$ is

$$D_t(\phi - \langle\phi\rangle) - \nabla_\perp \cdot D_t \nabla_\perp (2\phi - \langle\phi\rangle + T_i) + \partial_y \phi - \epsilon_n \hat{C}(2\phi - \langle\phi\rangle + T_i) + \epsilon_v \partial_\parallel v_\parallel = 0, \quad (1)$$

$$D_t\left[T_i - \frac{2}{3}(\phi - \langle\phi\rangle)\right] + \left(\eta_i - \frac{2}{3}\right)\partial_y \phi - \frac{5}{3}\epsilon_n \hat{C} T_i = \frac{2}{3}\kappa_i \partial_\parallel^2 T_i, \quad (2)$$

$$D_t v_\parallel = -\epsilon_v \partial_\parallel (2\phi + T_i). \quad (3)$$

It results from the ion density, temperature, and parallel velocity equations, respectively, including advection, polarization, and curvature drift, with the electron adiabaticity relation $n = \phi - \langle\phi\rangle$. The contributions from the flux surface average $\langle\phi\rangle$ assure that the electrons do not react adiabatically to ϕ fluctuations homogeneous on a flux surface, thus allowing for ZFs [2]. The background electron and ion temperatures are equal, and the ions are singly charged. Gradient lengths are defined as $L_\xi = d\ln r/d\ln\xi$, $\xi = n_0, T_{i0}$. The parallel coordinate, $z \equiv \theta$, ranges from $-\pi \ldots \pi$; i.e., the parallel length unit is $L_\parallel = qR$. The perpendicular coordinates, x, y, are given in terms of the ion gyroradius, $\rho_i = \sqrt{m_i T_{i0}}/(eB)$. The unit for the electric potential energy, $e\phi$, and the ion temperature is $T_{i0}\rho_i/L_n$. With the ion sound velocity, $c_s = \sqrt{T_{i0}/m_i}$, the parallel and perpendicular velocity unit is $v_{di} = c_s \rho_i / L_n$, which makes the time unit $t_0 = L_n/c_s$.

 0031-9007/04/93(6)/065001(4)$22.50

The dimensionless parameters are $\epsilon_n = 2L_n/R$, $\eta_i = L_n/L_{T_i}$, $\epsilon_v = \epsilon_n/(2q) = L_n/(qR)$ (the ion sound speed, c_s, in terms of $L_\parallel/t_0$, which differs from the parallel velocity unit), κ_i is the parallel heat conductivity. To obtain damping rates similar to those from kinetic phase mixing, κ_i for the $k_y = 0$ equilibrium perturbations (for the $k_y > 0$ turbulence modes) is chosen, so that temperature perturbations with a typical parallel wave number $k_\parallel = 1$ (~ 4 for the turbulence modes) are damped at the sound frequency, i.e., $\kappa_i = 3/2\epsilon_v$ ($\kappa_i = 3/8\epsilon_v$). The advective time derivative, D_t, is $\partial_t + (\hat{z} \times \nabla_\perp \phi) \cdot \nabla_\perp$, the curvature terms are taken for circular geometry, $\hat{C} = \cos z \partial_y + \sin z \partial_x$, and the derivative along the magnetic field, $\partial_\parallel$, is $\partial_z - sx\partial_y$, taking into account the magnetic shear s. The ITG modes in the above system have been examined in [11]. As discussed below, this model describes both the required ingredients, undamped stationary ZFs [3] and geodesic acoustic modes (GAM) [12,13].

Basic computational results.—A turbulence computation at the cyclone base case parameters [14], $\epsilon_n = 0.9$, $s = 0.8$, $R/L_n = 2.22$, $\eta_i = 3.1$, $q = 1.4$ may serve as reference. With the computational domain $130\rho_i \times 2000\rho_i \times 2\pi L_\parallel$, at a saturated anomalous heat diffusion coefficient $\chi_i = 1.7$ (unit $\rho_i^2 v_{th,i}/L_n$), agreeing reasonably well with the gyrokinetic result $\chi_i = 2.3$, the ZFs grow in nearly coherent structures up to a finite saturation value, as shown in Fig. 1. (For small domain widths in y, e.g., $130\rho_i \times 130\rho_i \times 2\pi L_\parallel$, the flows are more irregular, at somewhat reduced transport. This is a finite ρ^* effect due to the fluctuating part of the Reynolds stress [15].)

According to current wisdom, ZF saturation should be caused by a reduction of poloidal Reynolds stress $R_p = \langle v_{Ey}(v_{dix} + v_{Ex})\rangle$ (including the diamagnetic contribution [16]), where $v_{Ex} = -\partial_y \phi$, $v_{Ey} = \partial_x \phi$, $v_{dix} = -\partial_y(\phi - \langle\phi\rangle + T_i)$. However, the numerical stress continues to drive the flows, as seen in the lower half of Fig. 1 and in instantaneous plots of flow, shearing rate, and stress (solid plots in Fig. 2). By itself, the poloidal Reynolds stress would result in a high ZF growth rate of order 1.

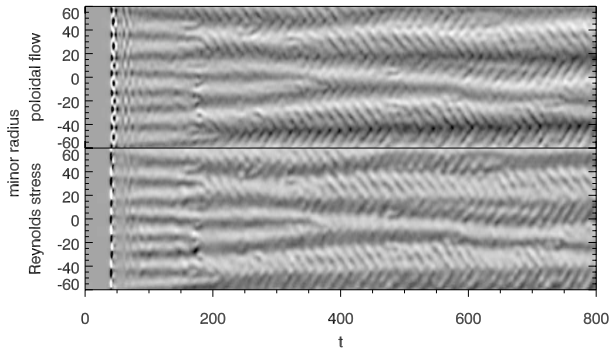

FIG. 1. Flux surface averages of poloidal flow $\langle v_{Ey}\rangle = \langle \partial_x \phi\rangle$ (upper plot) and perpendicular Reynolds stress $\langle v_{Ey}(v_{Ex} + v_{dix})\rangle$ (lower plot) versus minor radius and time. The stress is in phase with the flow shear, i.e., it is driving the flow. The superposed fast oscillations are (subdominant) GAMs.

Analysis of toroidal zonal flow drive.—To solve this seeming contradiction, it is necessary to reexamine the ZF drive, while taking into account toroidicity. First, let us verify the qualitative presence of the three flow eigenmodes of the kinetic system: For a stationary poloidal ZF, with $k_y = \omega = 0$, one obtains from the turbulence equations $T_i = 0$, $\phi = \langle\phi\rangle$, and $v_\parallel = -\epsilon_n/\epsilon_v \cos\theta \partial_x \phi = -2q\cos\theta v_{Ey}$, the return flow, which cancels the divergence of the poloidal flow [17]. The likewise stationary toroidal flow has the poloidal structure $v_\parallel(\theta) = \text{const}$ and $\phi = T_i = 0$. Both of these flow modes are undamped, which is required for a qualitative agreement with the exact kinetic behavior [3]. The last type of flow is the oscillating GAM, which in the limit $\kappa_i, \epsilon_v \to 0$ for radial wave numbers $k_x \ll 1$ has the poloidal mode structure $\phi = \langle\phi\rangle(1 + k_x \sin\theta/\omega)[1 + O(k_x^2)]$, $T_i = 2/3\langle\phi\rangle \times (k_x \sin\theta/\omega)[1 + O(k_x^2)]$, and frequency $\omega = 4/3\epsilon_n$. [12]. For the actually used κ_i and ϵ_v, the GAM frequency is shifted somewhat due to the coupling to the parallel velocity, and it is damped in about a sound transit time, as it is in the kinetic system by Landau damping [18].

The total kinetic energy density of the stationary ZF, including the return flow, is $E(v_y) = \langle v_\parallel^2\rangle/2 + \langle v_{Ey}^2\rangle/2 = (1 + 2q^2)\langle v_{Ey}\rangle^2/2$. Since in practical cases $q > 1$, the parallel flow represents the major part of the energy. Effectively, the poloidal flows exhibit a mass density enhanced by the factor $1 + 2q^2$ (collisionless $1 + 1.6q^2/\sqrt{\epsilon}$ at low inverse aspect ratio $\epsilon = a/R$ [3]), which has previously been noted in [17]. Combining the mode structure with energy conservation, one immediately obtains the rate of change of the ZFs, $\partial_t v_{Ey} = \langle f_y - 2q\cos(\theta) f_\parallel\rangle/(1 + 2q^2)$,

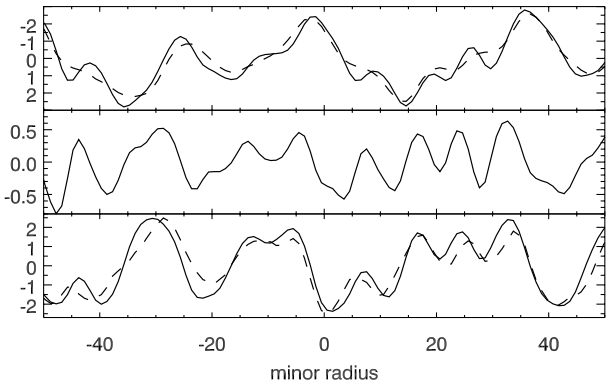

FIG. 2. Flux surface averages versus radius in dimensionless units at $t = 710$. Solid: poloidal flow $\langle v_{Ey}\rangle = \langle \partial_x \phi\rangle$ (upper plot), shearing rate $\langle \partial_x v_{Ey}\rangle = \langle \partial_x^2 \phi\rangle$ (middle plot), poloidal Reynolds stress $\langle v_{Ey}(v_{Ex} + v_{dix})\rangle$ (lower plot). Dashed: return flow $-q^{-1}\langle\cos\theta v_\parallel\rangle$ (upper plot), negative effective parallel stress $-2qR_\parallel = 2q\langle\cos\theta v_{Ex} v_\parallel\rangle$ (lower plot). Note the good balance between poloidal and parallel return flow and poloidal and parallel stress, respectively. The poloidal stress is in phase with the shearing rate and is thus driving.

with the poloidal and parallel force densities, $f_y, f_\parallel$. Apparently, the most important term is not the flux surface averaged poloidal force, $\langle f_y \rangle = -\partial_x R_p$, since it is weakened by the neoclassical factor, but instead the in/out asymmetry of the parallel force $\langle f_\parallel \cos\theta \rangle = -\partial_x R_\parallel$ produced by the appropriate average $R_\parallel = \langle \cos(\theta) v_\parallel v_{Ex} \rangle$ of the parallel Reynolds stress.

Purely poloidal flows have a high instability threshold and tend to be amplified by negative turbulence viscosity [4,19,20]. In contrast, the parallel ZF component becomes unstable at low velocities and experiences turbulent braking. Both effects can be derived from the linear response to a parallel momentum source $S_\parallel$ with $k_\parallel \neq 0$ in the presence of a sheared parallel background flow $v_{\parallel 0}$. For simplicity, we neglect the poloidal ZF component, Larmor radius effects, diamagnetic and curvature drifts, and assume the parallel heat conduction/kinetic phase mixing to render the temperature response unimportant ($T_i, k_x^2, \epsilon_n \to 0$). (These effects would shift the resonances by the diamagnetic and curvature drift frequencies.) The result is still qualitatively correct (and is corroborated by the computational studies shown below, which include the complete dynamics) because the main features of the parallel flows are their compressible dynamics and their interaction with the parallel sound wave. The linear response obeys the equations

$$\partial_t \phi + \epsilon_v \partial_\parallel v_\parallel = 0, \tag{4}$$

$$\partial_t v_\parallel - \partial_y \phi \partial_x v_{\parallel 0} + 2\epsilon_v \partial_\parallel \phi = S_\parallel, \tag{5}$$

with the frequency space solution

$$v_\parallel = R(\omega) S_\parallel = \frac{i\omega S_\parallel}{\omega^2 + k_y \epsilon_v k_\parallel \partial_x v_\parallel} - \omega_s^2, \qquad \omega_s^2 = 2\epsilon_v^2 k_\parallel^2. \tag{6}$$

The nonlinear turbulent mixing can be approximately taken into account by replacing ω by $\omega + i\Delta$, where $\Delta > 0$ is the decorrelation rate. The main purpose of the quantity Δ is thereby to select the appropriate integration paths in the complex plane in integrals involving R.

The complex resonances of the response $R(\omega)$ correspond to the flow instabilities. A growth rate $\sqrt{k_y \epsilon_v k_\parallel \partial_x v_\parallel} - \omega_s^2$ is obtained, provided the threshold $(\partial_x v_{\parallel 0})_{\rm crit} = 2\epsilon_v k_\parallel / k_y$ is exceeded for some pair $k_\parallel, k_y$. The threshold is lowest if $|k_y|$ is as high as possible, but Larmor radius effects require $|k_y| \ll 1$, while $|k_\parallel| \sim 1$ due to geometrical constraints. Using $|k_y| \approx 1/2$ as an order of magnitude estimate puts the threshold at $4\epsilon_v$, or converted into the poloidal velocity, assuming the mode structure of a stationary ZF,

$$(\partial_x v_{Ey0})_{\rm crit} \sim \frac{2\epsilon_v}{q} = \frac{\epsilon_n}{q^2}. \tag{7}$$

Because of the threshold, the instability should be localized preferably in the regions of highest shearing rate. (This is different from the tertiary instability found in [9], which is localized in the regions of lowest shearing rate/highest temperature gradient and is absent in the fluid system.)

Far below the threshold, for small instability drive $\partial_x v_{\parallel 0}$, a quasilinear estimate of the average turbulence viscosity $\mu_\parallel$ acting on the parallel component of a ZF is obtained by computing the time averaged parallel Reynolds stress $\overline{v_{Ex} v_\parallel} = -\mu_\parallel \partial_x v_{\parallel 0}$, taking the advective nonlinearity $-v_{Ex} \partial_x v_{\parallel 0}$ perturbatively as source $S_\parallel$,

$$\overline{v_{Ex} v_\parallel} = -\int d\omega d^3k |v_{Ex}(\omega, \mathbf{k})|^2 \partial_x v_{\parallel 0} \mathrm{Re}[R(\omega + i\Delta)], \tag{8}$$

$$\mathrm{Re}[R(\omega + i\Delta)] = \frac{\Delta(\omega^2 + \Delta^2 + \omega_s^2)}{(\omega^2 - \omega_s^2 - \Delta^2)^2 + 4\Delta^2\omega^2}. \tag{9}$$

The result is that the parallel turbulence viscosity is always positive. For parameters where the sound frequency is important (i.e., $\omega_s > \Delta, \omega$), it reduces the parallel momentum transport in comparison to the corresponding expression for the (negative) perpendicular viscosity [4], and yields $\mu_\parallel \propto \omega_s^{-2} \propto q^2$, favoring the excitation of ZFs for lower q.

Numerical study of toroidal effects.—The return flow strength $\langle v_\parallel \cos(\theta) \rangle$ in the turbulence computation agrees with the linear mode structure (Fig. 2, upper third). For the saturated flow state, the driving poloidal stress is exactly balanced by the braking in/out antisymmetric parallel Reynolds stress (lower part of Fig. 2), which explains the ZF saturation. Artificially eliminating the toroidicity induced ZF component by the replacement $\hat{C}(2\phi - \langle\phi\rangle) \to 2\hat{C}(\phi - \langle\phi\rangle)$, instead, leads to unsaturated growth of the ZFs, until the turbulence is essentially quenched. (This effect has been noted also in an unrelated study [21].) Apparently, there are no further significant flow damping effects in the fluid model.

To test whether the parallel stress is caused by a ZF instability, a turbulence computation without temperature and density gradient but with the ZFs artificially maintained at typical strength was carried out. The numerical instability threshold, $|v'_{Ey\rm crit}| = 0.5$, agrees with the estimate (7) and is close to the ITG computation's ZF saturation value (see Fig. 3). Even here, the perpendicular Reynolds stress is driving the flow, while the parallel one is braking it. However, the saturation level of the braking force is a factor of 5 lower than in the ITG computation. The quasilinear parallel turbulence viscosity of the regular ITG turbulence seems to dominate, since $\mu_\parallel$ is close to the anomalous heat diffusion coefficient, and the poloidal viscosity is about 4 times larger (at opposite sign). Furthermore, numerical experiments with artificially excited ZFs and ambient ITG turbulence confirm that $\mu_\parallel$ is essentially proportional to the turbulence intensity.

Different from the collisional case, with linearly undamped ZFs, the braking by parallel stress approaches

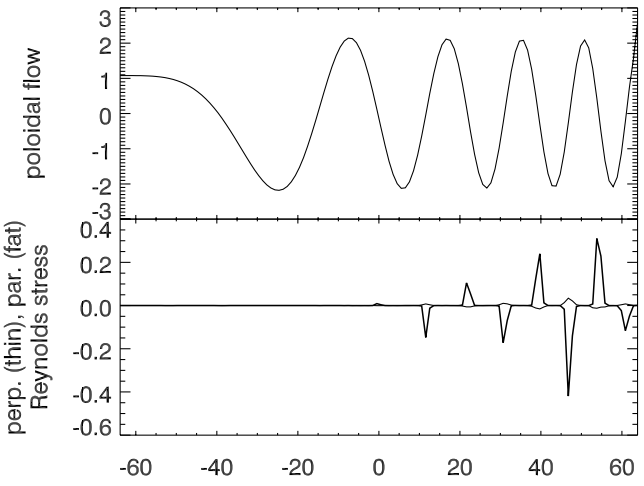

FIG. 3. Upper plot: flow profile used for the ZF instability simulation; lower plot: saturated flux surface averages of perpendicular Reynolds stress $\langle v_{Ey}(v_{Ex} + v_{\mathrm{dix}})\rangle$ (thin), and effective parallel stress $-2q\langle\cos\theta v_{Ex}v_{\parallel}\rangle$ (fat) in dimensionless units. The threshold poloidal flow shear at $x = 0$ is 0.5.

zero at decreasing turbulence intensity. Hence, the saturation amplitude of the ZFs should in general not tend to zero when the ITG modes are stabilized at some temperature gradient (if this is not prevented by a ZF instability [9]). Therefore, the ITG modes should be quenched at some point where the shearing rate exceeds the growth rate, before the actual threshold is reached. Indeed, analogous to gyrokinetic simulations [14], in the model system, the ZFs quench the transport completely, despite a linear ITG instability, as shown in Fig. 4.

Conclusions.—In all performed computations, the ratio of high-speed parallel flow to poloidal flow remains unchanged at the linear value, maintaining incompressibility. The ZFs are always driven by the poloidal turbulent stress. Saturation is obtained by the damping of the parallel flow component by parallel turbulent forces.

The parallel flow component can cause an instability at far lower threshold than the purely poloidal flows. However, the resulting saturated damping rate is too low to explain the damping in the full ITG driven system. In contrast, a quasilinear estimate of the parallel ITG turbulence viscosity agrees with the numerical results.

Since both the parallel viscosity (for low enough safety factor q) and the fraction of parallel flow energy are proportional to the square of the connection length along the magnetic field, increasing this length markedly reduces the ZF level at a concomitant rise in anomalous transport. Thus, safety factors of over about 3 completely suppress the stationary flows leaving only the oscillating geodesic acoustic modes [12]. Lowering q or an artificial elimination of the parallel ZF component enhances the ZF level at reduced or quenched transport.

All these facts suggest including the parallel flow dynamics in comprehensive analytical transport models, such as [4]. Moreover, an experimental measurement of

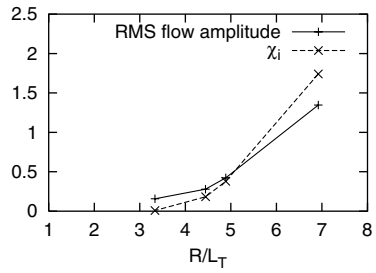

FIG. 4. Anomalous heat transport χ_i, rms shear flow from turbulence computations with varying temperature gradient in dimensionless units.

the forcing of the toroidicity-induced flow component, e.g., by similar methods as in [7,8], would seem very interesting. Last, the foregoing discussion is not restricted to tokamaks, but applies to all kinds of curved magnetic fields. Thus it might well prove relevant, e.g., in the treatment of solar coronal loops as soon as the research in this direction is sufficiently advanced to be interested in flows in these structures.

I would like to thank Professor K. Itoh for inspiring discussions and acknowledge the support of MEXT at NIFS.

[1] Z. Lin *et al.*, Phys. Plasmas **7**, 1857 (2000).
[2] G.W. Hammett *et al.*, Plasma Phys. Controlled Fusion **35**, 973 (1993).
[3] M. N. Rosenbluth *et al.*, Phys. Rev. Lett. **80**, 724 (1998).
[4] P. H. Diamond *et al.*, in Proceedings of the 17th IAEA Fusion Energy Conference, IAEA-CN-69/TH3/1, 1998.
[5] S. Champeaux and P. H. Diamond, Phys. Lett. A **288**, 214 (2001).
[6] K. Hallatschek and P. H. Diamond, New J. Phys. **5**, 29 (2003).
[7] C. Hidalgo *et al.*, Phys. Rev. Lett. **83**, 2203 (1999).
[8] R. A. Moyer *et al.*, Phys. Rev. Lett. **87**, 135001 (2001).
[9] B. N. Rogers, W. Dorland, and M. Kotschenreuther, Phys. Rev. Lett. **85**, 5336 (2000).
[10] K. Hallatschek and A. Zeiler, Phys. Plasmas **7**, 2554 (2000).
[11] A. Zeiler *et al.*, Phys. Plasmas **5**, 2654 (1998).
[12] K. Hallatschek *et al.*, Phys. Rev. Lett., **86**, 1223 (2001).
[13] T. S. Hahm *et al.*, Phys. Plasmas **6**, 922 (1999).
[14] A. M. Dimits *et al.*, Phys. Plasmas **7**, 969 (2000).
[15] K. Hallatschek, Phys. Rev. Lett., **84**, 5145 (2000).
[16] A. I. Smolyakov *et al.*, Phys. Plasmas **7**, 3987 (2000).
[17] K. Itoh and S. I. Itoh, Plasma Phys. Controlled Fusion **38**, 1 (1996).
[18] F. L. Hinton and M. N. Rosenbluth, Plasma Phys. Controlled Fusion **41**, A653 (1999).
[19] A. V. Chechkin *et al.*, Zh. Eksp. Teor. Fiz. **113**, 646 (1998) [Sov. Phys. JETP **86**, 357 (1998)].
[20] L. Chen, Z. Lin, and R. B. White, Phys. Plasmas **7**, 3129 (2000).
[21] H. Sugama, T. H. Watanabe, and W. Horton, Phys. Plasmas **10**, 726 (2003).